**Jurnal Rivet (Riset dan Invensi Teknologi)**
Program Studi Teknik Sipil-Universitas Dharma Andalas
Vol.06 No.01 Juni 2026

# Integrated Geoelectric-Geotechnical Characterization For Landslide Mitigation In East Kalimantan, Indonesia

**Aco Wahyudi Efendi** [1*]

1) Doktoral Teknik Sipil, Universitas Sebelas Maret Surakarta-Universitas Sebelas Maret (acowahyudiefendi@student.uns.ac.id)

***Info Artikel***
***Riwayat Artikel:***
*Dikirim :30-05-2026*
*Direvisi :15-06-2026*
*Diterima : 30-06-2026*

***Keywords :***
*Geotechnical, Geoelectric Resistivity, Landslide Investigation, Standard Penetration Test (SPT), Test Pit Excavation.*

**ABSTRACT**

A significant landslide affecting Syarifuddin Yoes Road in the Kutai Basin, East Kalimantan, was triggered by elevated pore water pressure from leaking PDAM water infrastructure and inadequate surface drainage. This investigation integrated two-dimensional (2D) geoelectric resistivity surveys (Schlumberger configuration), Standard Penetration Tests (SPT), and visual inspection from 4-meter-deep test pits to characterize the 60-meter rotational failure mechanism. Visual analysis revealed a continuous soil flow. A robust inverse correlation was established: low-resistivity anomalies (1–50 Ohm-m) directly corresponded with low SPT N-values (2–8 blows/30 cm) and weak saturated clays. Borehole data detected groundwater at 4 meters, aligning with low-resistivity anomalies at 4.5 meters. This multi-method approach successfully identified the primary weak slip surface at a depth of 5 to 8 meters. The geoelectric method is recommended as an efficient, cost-effective initial benchmark for spatial subsurface characterization before costly intrusive boring. These integrated subsurface models substantiated the design of D600 Contiguous Bored Piles as a mitigation structure.

## 1. INTRODUCTION

Land subsidence and rotational landslides represent some of the most destructive geological hazards, frequently resulting in catastrophic infrastructure failure and economic loss. A landslide, fundamentally defined as the downward movement of earth materials under the influence of gravity, is governed by a complex interplay of active and passive factors, predominantly geology, geomorphology, hydrogeology, and external loading conditions (Al-Heety et al., 2020; Anderson & Brown, 2019; Baker et al., 2018; Blum et al., 2017; Chambers et al., 2014; Cuttler et al., 2018; Dahlin & Zhou, 2004; A. W. Efendi, 2016; Ferhat et al., 2022; Fikos et al., 2012; Godio et al., 2019; Goldman & Kafri, 2020; Hana et al., 2021; Hunt, 2005; Ismail et al., 2021; Jain & Singh, 2020; Kamshilin & Kaznacheev, 2018; Kearey et al., 2002; Loke & Barker, 1996; Love et al., 2018; Milsom, 2003; Naudet et al., 2008; Osazuwa & Chinedu, 2019; Palacky, 1987; Perrone et al., 2014; Reynolds, 2011; Safani et al., 2005; Sanchaa et al., 2019; Sumanovac & Weisser, 2001; Ward, 1990; Woodroffe, 2019). In the context of East Kalimantan, specifically within the Kutai Basin, the prevalence of the Balikpapan Formation—characterized by interbedded sandstone, clay, and shale—creates a naturally susceptible environment for slope instability (Dahlin & Zhou, 2004; Supriatna et al., 1995; Van Bemmelen, 1949; Zhou et al., 2017).

The limitation of conventional geotechnical boring is that it only provides highly localized point data, often missing the lateral extent of subsurface anomalies. Conversely, geoelectric resistivity surveys offer a continuous two-dimensional profile of the subsurface but require ground-truthing to accurately assign lithological names to resistivity values (Al-Heety et al., 2020; Anderson & Brown, 2019; Baker et al., 2018;

Blum et al., 2017; Chambers et al., 2014; Cuttler et al., 2018; Dahlin & Zhou, 2004; A. W. Efendi, 2016; Ferhat et al., 2022; Fikos et al., 2012; Godio et al., 2019; Goldman & Kafri, 2020; Hana et al., 2021; Hunt, 2005; Ismail et al., 2021; Jain & Singh, 2020; Kamshilin & Kaznacheev, 2018; Kearey et al., 2002; Loke & Barker, 1996; Love et al., 2018; Milsom, 2003; Naudet et al., 2008; Osazuwa & Chinedu, 2019; Palacky, 1987; Perrone et al., 2014; Reynolds, 2011; Safani et al., 2005; Sanchaa et al., 2019; Sumanovac & Weisser, 2001; Ward, 1990; Woodroffe, 2019). Therefore, correlating geoelectric data with SPT and test pit visual logs bridges the gap between extensive geophysical mapping and precise geotechnical quantification. This study focuses on STA 3+634 on the Syarifuddin Yoes route, where a 60-meter rotational landslide has severely damaged the road structure, tilted utility poles, and cracked masonry. The objective is to delineate the slip surface by correlating 2D resistivity imaging with borehole and test pit data, ultimately verifying the mechanism of failure driven by a leaking PDAM pipe and inadequate drainage, to propose structurally sound mitigation measures shown in figure 1.

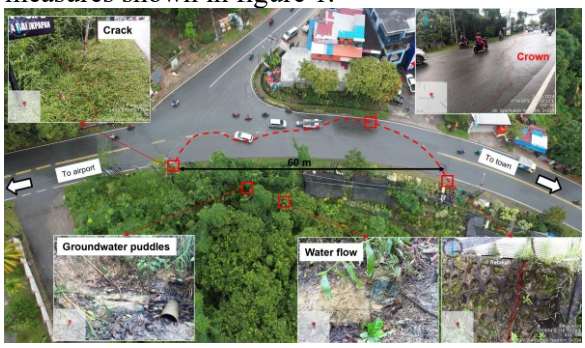


**Figure 1.** Research location

## 2. METHOD

### 2.1. Study Area and Geological Setting

The investigation site is situated at STA 3+634 in Balikpapan, falling within the physiographic zone of the Kutai Basin. Based on the Samarinda Geological Sheet, the local stratigraphy comprises the Balikpapan Formation (Tmbp), which consists of alternating quartz sandstone, claystone, siltstone, shale, and coal seams (Dahlin & Zhou, 2004; A. W. Efendi, 2023b, 2024; Supriatna et al., 1995; Van Bemmelen, 1949; Zhou et al., 2017). The morphological setting is a hilly terrain at an elevation of approximately 175 meters above sea level. The specific landslide event is classified as a rotational slide spanning 60 meters in width, oriented at 357° N, with an 8% slope gradient. Field observations indicate that the superelevation of the road channels surface runoff directly into the landslide zone, while a leaking underground PDAM pipe at the slope toe has saturated the subsoil.

### 2.2. Geoelectric Resistivity Survey

The geoelectric investigation utilized the resistivity method based on the Schlumberger configuration, selected for its superior vertical sounding capabilities and sensitivity to horizontal changes in clay and water content (A. W. Efendi, 2022, 2023a; AW. E. W. A. W. Efendi, 2019a, 2019e, 2019d, 2019c, 2019b Al-Heety et al., 2020; Anderson & Brown, 2019; Baker et al., 2018; Blum et al., 2017; Chambers et al., 2014; Cuttler et al., 2018; Dahlin & Zhou, 2004; A. W. Efendi, 2016; Ferhat et al., 2022; Fikos et al., 2012; Godio et al., 2019; Goldman & Kafri, 2020; Hana et al., 2021; Hunt, 2005; Ismail et al., 2021; Jain & Singh, 2020; Kamshilin & Kaznacheev, 2018; Kearey et al., 2002; Loke & Barker, 1996; Love et al., 2018; Milsom, 2003; Naudet et al., 2008; Osazuwa & Chinedu, 2019; Palacky, 1987; Perrone et al., 2014; Reynolds, 2011; Safani et al., 2005; Sanchaa et al., 2019; Sumanovac & Weisser, 2001; Ward, 1990; Woodroffe, 2019). The IPMGEO-4100 instrument was employed, which measures both apparent resistivity and induced polarization (chargeability). The device injects a square-pulsed DC current (max 400V, 100mA) through current electrodes (AB) and measures the resulting potential difference through potential electrodes (MN) shown in figure 2. Data acquisition involved systematically increasing the AB/2 spacing to achieve a depth penetration exceeding 20 meters, with MN/2 adjustments kept strictly within 1/5 of the AB/2 distance to maintain data fidelity and minimize spontaneous potential noise. Apparent resistivity (ρa) was calculated using the geometric factor (K) for the Schlumberger array:

$$\rho a = K\left(\frac{\Delta V}{I}\right) \qquad (1)$$

where

$$K = \pi \frac{(\frac{AB}{2})^2 - (\frac{MN}{2})^2}{MN} \quad (2)$$

The raw data were processed via curve matching and inverse modeling to generate a 2D pseudo-section.

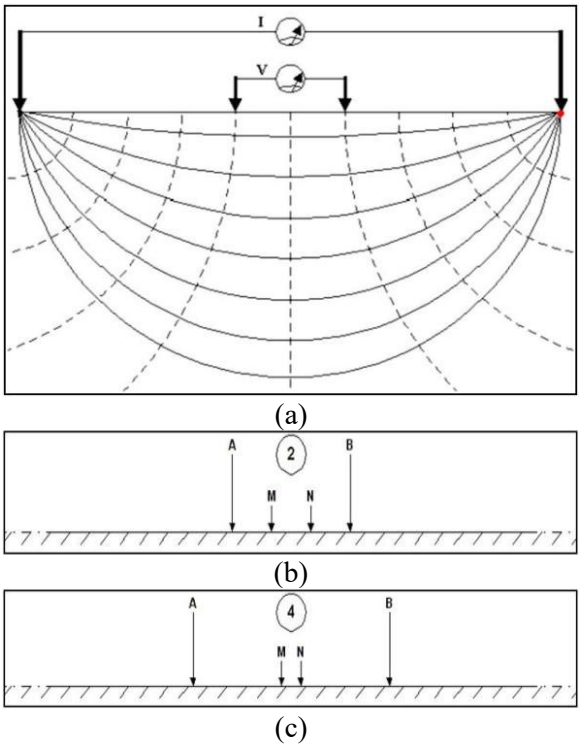


**Figure 2.** (a) Geoelectric working method concept (b) Wenner Configuration (c) Schlumberger Configuration

### 2.3. Geotechnical Investigation (Boring and SPT)

To validate the geoelectric profiles, two boreholes (BH-01 and BH-02) were drilled to a depth of 20 meters. Standard Penetration Tests (SPT) were conducted at regular 1.5-meter intervals using a 63.5 kg hammer dropped from 760 mm, adhering to SNI 8460:2017. The SPT N-value (blows per 30 cm penetration) provides a direct empirical measure of soil stiffness and shear strength, essential for identifying the weak zones indicative of a slip surface. Disturbed and undisturbed samples were collected for visual classification and laboratory testing, as shown in Figure 3.

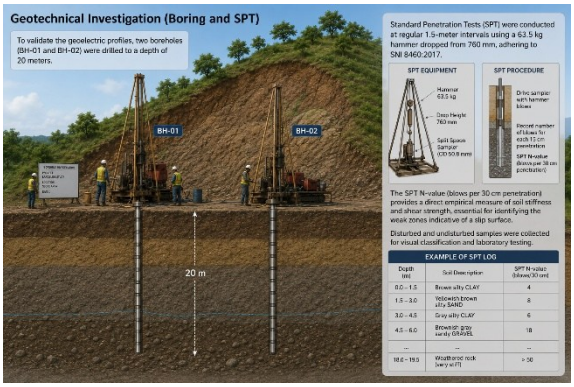


**Figure 3.** Geotechnical Investigation (Boring and SPT)

### 2.4. Test Pit Excavation

A visual inspection pit was excavated to a depth of 4 meters near the crown and mid-slope of the landslide. This method allows for direct, high-resolution observation of the soil profile, fracture patterns, and water seepage zones that are often smeared or lost during rotary boring. The visual logs from the test pit were categorized based on soil color, texture, moisture content, and structural integrity, as shown in Figure 4.

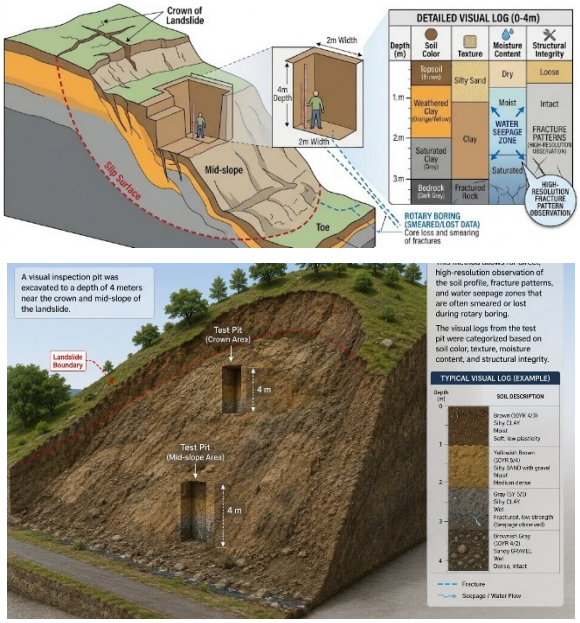


**Figure 4.** A visual inspection pit excavation

## 3. RESULTS AND DISCUSSION

### 3.1. Geoelectric Resistivity Findings

The 2D resistivity inversion model along the landslide profile successfully mapped three

distinct subsurface zones. The shallowest layer, extending from the surface to a depth of approximately 2 to 4 meters, exhibited moderate resistivity values ranging from 100 to 300 Ohm-m. Based on the reference table for common rocks and minerals, these values correspond to moderately dry topsoil and loose sand. The second layer, located between depths of 4 and 9 meters, displayed very low resistivity values, predominantly between 1 and 50 Ohm-m. This zone laterally underlies the failed road section and dips toward the toe. Such low resistivity is a classic indicator of water-saturated, high-plasticity clay or weathered shale. The third layer, underlying the low-resistivity zone at depths greater than 9 meters, showed a significant increase in resistivity (500–2000 Ohm-m), interpreted as competent, unweathered sandstone and greenstone bedrock. The geometry of the low-resistivity second layer forms a concave shape, geometrically consistent with a rotational slip surface shown in figure 5 (Al-Heety et al., 2020; Anderson & Brown, 2019; Baker et al., 2018; Chambers et al., 2014; Dahlin & Zhou, 2004; Fikos et al., 2012; Godio et al., 2019; Hunt, 2005; Ismail et al., 2021; Jain & Singh, 2020; Kearey et al., 2002; Loke & Barker, 1996; Milsom, 2003; Naudet et al., 2008; Osazuwa & Chinedu, 2019; Palacky, 1987; Perrone et al., 2014; Reynolds, 2011; Safani et al., 2005; Sumanovac & Weisser, 2001; Ward, 1990).


**Figure 5.** Geoelectric Data Results for Syarifudin Yoes Street, Station 3+634

### 3.2. Borehole and SPT Results

The stratigraphic logs from BH-01 and BH-02 corroborate the geophysical interpretations. BH-01, located near the crown, revealed 3 meters of silty sand overlying 6 meters of soft, dark grey, high-plasticity clay, resting on dense sandstone. BH-02, situated near the toe, showed a thicker accumulation of soft clay (up to 8 meters), indicating the accumulation of the slide mass. The SPT N-values provide quantitative evidence of the weak zone. In the upper sandy layer, N-values ranged from 15 to 25 blows/30 cm. However, within the 4 to 9-meter depth interval, the SPT N-values plummeted drastically to 2–8 blows/30 cm, often yielding "weight of hammer" (WoH) conditions in highly remolded zones. Below 9 meters, the N-values exceeded 50

blows/30 cm, confirming the competent bedrock shown in Figure 6.

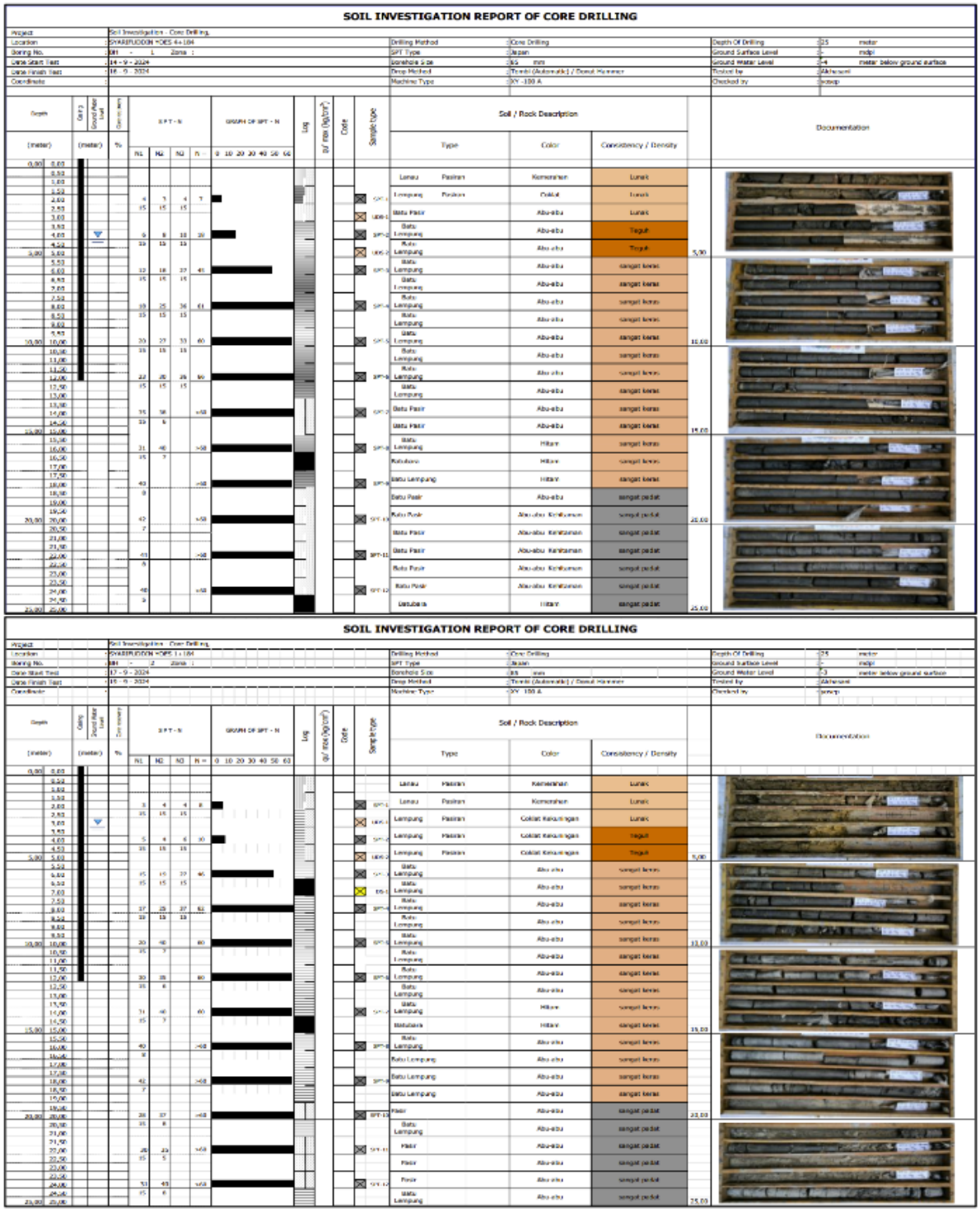


Figure 6. Landslide Drilling Data Results for Syarifudin Yoes Street, Station 3+634

### 3.3. Test Pit Visual Observations

The 4-meter test pit excavation provided critical visual evidence of the failure mechanism. The upper 1.5 meters consisted of brown, loose, silty sand with localized pockets of water. Between 1.5 and 4 meters, the soil transitioned into a dark grey, highly plastic, intensely slickensided clay. The clay appeared completely saturated, with visible seepage inflow from the eastern wall of the pit. The presence of slickensides (polished and striated shear surfaces) is direct visual confirmation of historical and ongoing shear deformation along the slip plane. The water encountered at this depth strongly supports the hypothesis that the leaking PDAM pipe is artificially charging the subsurface, as shown in Figure 7.

**Figure 7.** Test Pit Visual Observations

### 3.4. Correlation of Geoelectric, SPT, and Test Pit Data

The integration of these three distinct datasets establishes a high-confidence subsurface model. Table 1 summarizes the direct correlation between the measured resistivity, SPT N-values, and visual pit descriptions at equivalent depths.

**Table 1:** Correlation of Geoelectric, SPT, and Test Pit Data

| Depth (m) | Resistivity (Ohm-m) | SPT N-value (blows/30 cm) | Test Pit Visual Description | Lithological Interpretation | Slope Stability Implication |
|---|---|---|---|---|---|
| 0.0 – 1.5 | 150 – 300 | 15 – 25 | Brown, loose silty sand, slightly moist | Topsoil / Loose Sand (Overburden) | Stable under unsaturated conditions |
| 1.5 – 4.0 | 50 – 100 | 8 – 12 | Greyish brown sandy clay, moderate moisture | Weathered transition zone | Moderate strength, potential perching layer |
| 4.0 – 9.0 | 1 – 50 | 2 – 8 (WoH) | Dark grey, highly plastic, saturated clay with slickensides | Saturated Clay / Weathered Shale | Critical Weak Zone / Active Slip Surface |
| > 9.0 | 500 – 2000 | > 50 | Could not excavator; borehole shows dense grey sandstone | Competent Sandstone Bedrock | Stable stratum / Impermeable base |

The data in Table 1 clearly demonstrate that the low-resistivity anomaly (1–50 Ohm-m) aligns perfectly with the depth interval where the SPT N-values drop below 10 and where the test pit reveals saturated, slickensided clay. This convergence proves that the geoelectric method is highly sensitive to the geotechnical weakness and hydrological saturation of the slip surface (Al-Heety et al., 2020; Anderson & Brown, 2019; Baker et al., 2018; Chambers et al., 2014; Dahlin & Zhou, 2004; Fikos et al., 2012; Godio et al., 2019; Hunt, 2005; Ismail et al., 2021; Jain & Singh, 2020; Kearey et al., 2002; Loke & Barker, 1996; Milsom, 2003; Naudet et al., 2008;

Osazuwa & Chinedu, 2019; Palacky, 1987; Perrone et al., 2014; Reynolds, 2011; Safani et al., 2005; Sumanovac & Weisser, 2001; Ward, 1990).

**Table 2:** Summary of Test Data and Investigation Results for Landslide Mechanism

| Parameter | Investigation Result | Source / Method | Interpretation |
|---|---|---|---|
| Landslide Type | Rotational Slide | Field Observation & Resistivity | Concave slip surface confirmed by geometry |
| Slide Mass Volume | ~60 m wide, 7m depth | SPT & Geoelectric | Failure extends to 9m depth, accumulating at the toe |
| Pore Water Pressure | Critically High | Test Pit Seepage & Low Resistivity | PDAM leak and poor drainage saturate the clay |
| Shear Strength | Severely Reduced | SPT N-value = 2-8 | Remolded clay with zero effective cohesion |
| Factor of Safety (FoS) | < 1.0 (Unstable) | SNI 8460:2017 | Requires structural intervention to achieve FoS > 1.5 |

Landslide Mechanism and Mitigation Discussion
The mechanism of failure at STA 3+634 is a classic example of a rainfall-induced and anthropogenically exacerbated rotational slide. The Balikpapan formation naturally contains weak, smectitic clay layers. However, the primary triggering mechanism was the combination of the superelevated road geometry, which channeled surface water directly into the slope, and the leaking PDAM pipe at the toe. This constant influx of water infiltrated the weathered shale/clay layer (4–9m depth) shown in Figure 8. As the soil transitioned from an unsaturated to a fully saturated state, matric suction was lost, and pore water pressure increased dramatically. Consequently, the effective shear strength of the soil dropped below the driving gravitational forces, initiating the rotational slip along the low-resistivity, low-SPT zone.

**Figure 8.** The condition of the soil is saturated with water, according to geoelectric results there are pockets of water at that depth.

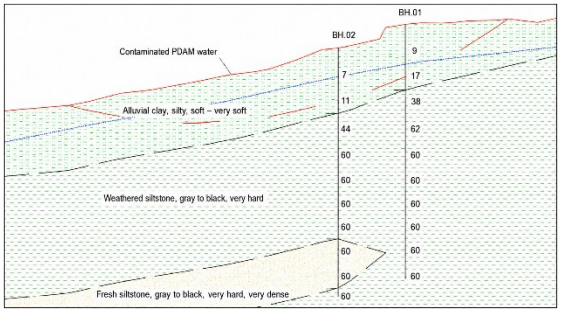


**Figure 9.** Soil stratigraphy and groundwater elevation

Given the depth of the slip surface (7–9 meters) and the need for a minimum Factor of Safety (FoS) of 1.5 as per SNI 8460:2017, superficial slope re-grading is insufficient. The investigation supports the implementation of deep structural mitigation shown in Figure 9.
Two alternatives were evaluated: Alternative 1 involves Deep Mixing Piles (DPT) combined with Bored Piles (D600), while Alternative 2 proposes a Contiguous Bored Pile (D600 mm) wall. The contiguous bored pile is highly recommended as it penetrates through the low-resistivity weak zone (4- 9 m) and sockets into the high-resistivity bedrock (> 9 m), providing sufficient structural rigidity to resist the lateral thrust of the saturated clay mass. Furthermore, the PDAM pipe must be repaired, and a comprehensive surface and subsurface drainage system must be installed to lower the pore water pressure, effectively increasing the resistivity and shear strength of the soil over time, as shown in Figure 10.

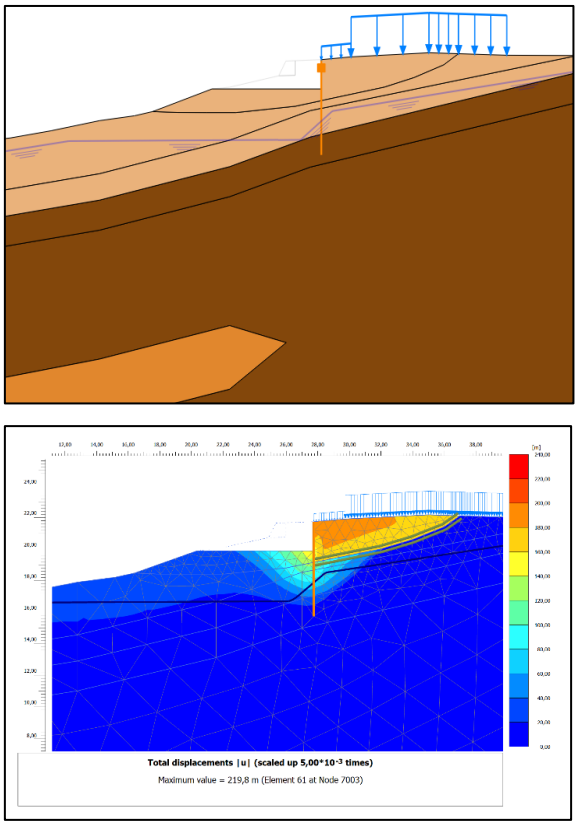


**Figure 10.** Geotechnical simulation analysis

## 4. CONCLUSION

The detailed investigation at STA 3+634 successfully demonstrates the efficacy of integrating geoelectric resistivity surveys with conventional geotechnical boring (SPT) and test pit excavations. The 2D resistivity imaging accurately identified the lateral extent and depth of a low-resistivity anomaly (1–50 Ohm-m), which correlated flawlessly with the severely low SPT N-values (2–8 blows/30 cm) and the visual presence of saturated, slickensided clay at depths between 4 and 9 meters. This multi-method approach eliminated the ambiguities inherent in using any single investigation method, providing a reliable subsurface model. The rotational landslide was confirmed to be triggered by water infiltration from a leaking PDAM pipe and poor road drainage, which saturated the weak clay layer of the Balikpapan Formation.

To ensure long-term stability and meet the safety factors mandated by SNI 8460:2017, the implementation of a D600 Contiguous Bored Pile system socketed into the competent bedrock, alongside rigorous hydrological management, is imperative. This integrated framework should be adopted for similar geotechnical hazard assessments in the Kutai Basin and other complex geological regions.

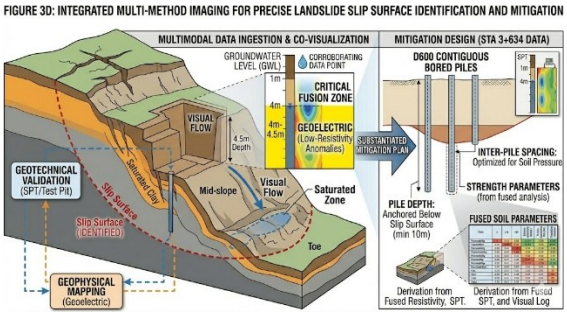


**Figure 11.** Integrated Geoelectric-Geotechnical Characterization

Visual analysis presented in Figure 8 identifies a continuous soil flow mechanism, a finding further corroborated by intrusive data. Specifically, a proximate SPT boring log encountered a stable groundwater table at 4 meters, which aligns precisely with high-resolution geoelectric profiles showing low-resistivity anomalies at 4.5 meters, indicative of saturated conditions and discrete water pockets. Based on this robust correlation, the geoelectric method is recommended as an effective, efficient, and cost-comparative benchmark for initial subsurface soil characterization, providing critical spatial data before more costly and time-consuming investigative methods.

## REFERENCE

Al-Heety, E. A., Al-Shuhail, A. A., & Bagash, F. K. (2020). Integration of electrical resistivity tomography and geotechnical methods for subsurface characterization. *Journal of Applied Geophysics*, *178*, 104053.

Anderson, D. L., & Brown, R. L. (2019). *Geotechnical and geophysical integration for landslide assessment*. Springer.

Baker, H. A., Ghnellawi, A. M., & Al-Shuhail, A. A. (2018). Correlation of electrical resistivity with standard penetration test for soil characterization. *Environmental Earth Sciences*, *77*(10), 1–12.

Blum, C. C., White, T. C., Sauter, E. A., Stewart, D. C., Bedrosian, P. A., & Love, J. J. (2017).

Geoelectric monitoring at the Boulder magnetic observatory. *Geoscientific Instrumentation, Methods and Data Systems*, *6*(2), 447–452. https://doi.org/10.5194/gi-6-447-2017

Chambers, J. E., Wilkinson, P. B., Kuras, O., Ford, J. R., Gunn, D. A., Meldrum, P. I., Ogilvy, R. D., & others. (2014). Three-dimensional geophysical anatomy of an active landslide in Liassic clays. *Geomorphology*, *213*, 279–294.

Cuttler, S. W., Love, J. J., & Swidinsky, A. (2018). Geoelectric hazard assessment: the differences of geoelectric responses during magnetic storms within common physiographic zones. *Earth, Planets and Space*, *70*(1). https://doi.org/10.1186/s40623-018-0807-7

Dahlin, T., & Zhou, B. (2004). A numerical comparison of 2D resistivity imaging with 10 electrode arrays. *Geophysical Prospecting*, *52*(5), 379–398.

Efendi, A. W. (2016). *Laporan Hasil Investigasi Rona Lapisan Tanah pada Situs Gunung Selendang Sanga-Sanga.*

Efendi, A. W. (2022). Geoelectric Methods to Determine the Location of Old Graves. *Bulletin of Computer Science and Electrical Engineering*, *3*(1), 30–39. https://doi.org/10.25008/bcsee.v3i1.1147

Efendi, A. W. (2023a). Availability of the Sangatta Pelangi Hill Slide Using Geoelectric Correlation on the Borlog. *Journal of Science and Education Research*. http://jurnal.insanmulia.or.id/index.php/jser/article/view/27

Efendi, A. W. (2023b). The Settlement Behavior Using Replacement Embankment with Mortar Foam and Geofoam using LISA FEA. *Nusantara Civil Engineering Journal*. http://ojs.poltekba.ac.id/ojs/index.php/nuce/article/view/484

Efendi, A. W. (2024). ChatGPT application in ground settlement analysis using LISA V. 8 FEA. *Research of Scientia Naturalis*. https://journal.ypidathu.or.id/index.php/scientia/article/view/826

Efendi, AW. E. W. A. W. (2019a). *Soil Investigation-Georesistant, Area Perumahan Kampung Timur Balikpapan*. Center for Open Science. https://doi.org/10.31227/osf.io/4zp5g

Efendi, AW. E. W. A. W. (2019b). *Soil Investigation-Georesistant, Landslide Desa Rerawah L=75 m Muara Teweh Kalteng*. Center for Open Science. https://doi.org/10.31227/osf.io/t673b

Efendi, AW. E. W. A. W. (2019c). *Soil Investigation-Georesistant, Landslide DPU Muara Teweh L=45 m Kalimantan Tengah*. Center for Open Science. https://doi.org/10.31227/osf.io/dbxq2

Efendi, AW. E. W. A. W. (2019d). *Soil Investigation-Georesistant, Landslide Komatsu L=52 m Hydroponic Balikpapan*. Center for Open Science. https://doi.org/10.31227/osf.io/qguws

Efendi, AW. E. W. A. W. (2019e). *Soil Investigation-Georesistant, Landslide Komatsu L=250 m Balikpapan*. Center for Open Science. https://doi.org/10.31227/osf.io/5mfwg

Ferhat, A., Seizarsyah, T., Bimantio, M. P., Nugraha, N. S., Putra, D. P., Suparyanto, T., Hidayat, A. A., & Pardamean, B. (2022). A Geoelectric Approach for Karst Groundwater Analysis. *IOP Conference Series: Earth and Environmental Science*, *998*(1), 12012. https://doi.org/10.1088/1755-1315/998/1/012012

Fikos, I., Zianou, A., & Tsourlos, P. (2012). Geoelectric investigation of a landslide: Correlation with geotechnical data. *Bulletin of Engineering Geology and the Environment*, *71*(1), 113–120.

Godio, A., Strobbia, C., & De Bacco, G. (2019). Geophysical characterization of a landslide: Resistivity and seismic surveys. *Engineering Geology*, *252*, 1–15.

Goldman, M., & Kafri, U. (2020). Geoelectric, Geoelectromagnetic and Combined Geophysical Methods in Groundwater Exploration in Israel. *Springer Hydrogeology*, 299–393. https://doi.org/10.1007/978-3-030-51148-7_16

Hana, G., Klanica, R., Stejskalová, Š., & Šteffl, J. (2021). Geoelectric, Magnetic Susceptibility and Geochemical Survey as a Tool to Clarify the Origin of Bronze Age Water Reservoirs at the Hillfort Štěpánov,

Czechia. *SSRN Electronic Journal*. https://doi.org/10.2139/ssrn.3950158

Hunt, R. E. (2005). *Geotechnical engineering investigation handbook* (2nd ed.). CRC Press.

Ismail, M. R., Usman, M., & Sulaiman, A. (2021). Landslide investigation using 2D electrical resistivity and geotechnical methods in East Kalimantan. *Landslides*, *18*(4), 1351–1363.

Jain, P., & Singh, R. (2020). Correlation between electrical resistivity and soil strength properties. *Geotechnical and Geological Engineering*, *38*(3), 2747–2759.

Kamshilin, A. N., & Kaznacheev, P. A. (2018). Local Current Gauge: Instrument for Geoelectric Measurements. *Seismic Instruments*, *54*(5), 573–578. https://doi.org/10.3103/s0747923918050079

Kearey, P., Brooks, M., & Hill, I. (2002). *An introduction to geophysical exploration* (3rd ed.). Blackwell Science.

Loke, M. H., & Barker, R. D. (1996). Rapid least-squares inversion of apparent resistivity pseudosections by a quasi-Newton method. *Geophysical Prospecting*, *44*(1), 131–152.

Love, J. J., Lucas, G. M., Kelbert, A., & Bedrosian, P. A. (2018). Geoelectric Hazard Maps for the Pacific Northwest. *Space Weather*, *16*(8), 1114–1127. https://doi.org/10.1029/2018sw001844

Milsom, J. (2003). *Field geophysics* (3rd ed.). John Wiley & Sons.

Naudet, V., Lazzari, M., & Morelli, G. (2008). Geophysical surveys for the characterization of landslides. *Engineering Geology*, *100*(1–2), 1–15.

Osazuwa, I. B., & Chinedu, A. D. (2019). Electrical resistivity tomography and geotechnical investigation of a highway failure. *Journal of African Earth Sciences*, *151*, 14–25.

Palacky, G. J. (1987). Resistivity characteristics of geologic targets. In M. N. Nabighian (Ed.), *Electromagnetic methods in applied geophysics* (Vol. 1, pp. 53–129). Society of Exploration Geophysicists.

Perrone, A., Lapenna, V., & Piscitelli, S. (2014). Electrical resistivity tomography technique for landslide investigation: A review. *Earth-Science Reviews*, *135*, 65–82.

Reynolds, J. M. (2011). *An introduction to applied and environmental geophysics* (2nd ed.). John Wiley & Sons.

Safani, A., Mazzotti, A., & Przyborska, M. (2005). 2D resistivity imaging of a landslide: A case study. *Near Surface Geophysics*, *3*(4), 215–224.

Sanchaa, A., Nevedrova, N., Shaparenko, I., Shalaginov, A., & Babushkin, S. (2019). Geoelectric Structure Of The Uimon Basin According To Ground Geoelectric. *Interexpo GEO-Siberia*, *2*(2), 137–144. https://doi.org/10.33764/2618-981x-2019-2-2-137-144

Sumanovac, F., & Weisser, M. (2001). Evaluation of resistivity and seismic methods for hydrogeological mapping in karst terrains. *Journal of Applied Geophysics*, *47*(1), 13–28.

Supriatna, S., Rustandi, E., & Wikarno. (1995). *Geological map of the Samarinda sheet, Kalimantan*. Geological Research and Development Centre.

Van Bemmelen, R. W. (1949). *The geology of Indonesia* (Vol. 1A). Government Printing Office.

Ward, S. H. (1990). Resistivity and induced polarization methods. In S. H. Ward (Ed.), *Geotechnical and environmental geophysics* (Vol. 1, pp. 147–189). Society of Exploration Geophysicists.

Woodroffe, J. R. (2019). Geoelectric Field Generation by Field-Aligned Currents. *Geomagnetically Induced Currents from the Sun to the Power Grid*, 79–92. https://doi.org/10.1002/9781119434412.ch5

Zhou, W., Beck, B. F., & Adams, A. L. (2017). Effective electrode configuration for the detection of sinkholes using 2D electrical resistivity tomography. *Pure and Applied Geophysics*, *159*(6), 1351–1367.